

Charge-Density Wave Order on a π -flux Square Lattice

Y.-X. Zhang,¹ H.-M. Guo,² and R. T. Scalettar¹

¹*Department of Physics, University of California, Davis, CA 95616, USA*

²*Department of Physics, Key Laboratory of Micro-nano Measurement-Manipulation and Physics (Ministry of Education), Beihang University, Beijing, 100191, China*

(Dated: June 18, 2022)

The effect of electron-phonon coupling (EPC) on Dirac fermions has recently been explored numerically on a honeycomb lattice, leading to precise quantitative values for the finite temperature and quantum critical points. In this paper, we use the unbiased determinant Quantum Monte Carlo (DQMC) method to study the Holstein model on a half-filled staggered-flux square lattice, and compare with the honeycomb lattice geometry, presenting results for a range of phonon frequencies $0.1 \leq \omega \leq 2.0$. We find that the interactions give rise to charge-density wave (CDW) order, but only above a finite coupling strength λ_{crit} . The transition temperature is evaluated and presented in a T_c - λ phase diagram. An accompanying mean-field theory (MFT) calculation also predicts the existence of quantum phase transition (QPT), but at a substantially smaller coupling strength.

I. INTRODUCTION

The physics of massless Dirac points, as exhibited in the band structure of the honeycomb lattice of graphene, has driven intense study[1–4]. The square lattice with π -flux per plaquette is an alternate tight-binding Hamiltonian which also contains Dirac points in its band structure. Initial investigations of the π -flux model focused on the non-interacting limit[5], but, as with the honeycomb lattice, considerable subsequent effort has gone into extending this understanding to incorporate the effect of electron-electron interactions. Numerical simulations of the Hubbard Hamiltonian with an on-site repulsion U between spin up and spin down fermions, including Exact Diagonalization [6] and Quantum Monte Carlo (QMC)[7–14] revealed a quantum phase transition at $U_c \sim 5.55t$ into a Mott antiferromagnetic (AF) phase in the chiral Heisenberg Gross-Neveu universality class. For a spinless fermion system with near-neighbor interactions a chiral Ising Gross-Neveu universality class is suggested[15]. These results have been contrasted with those on a honeycomb lattice, which has a similar Dirac point structure, though at a smaller critical interaction $U_c \sim 3.85t$ [11].

In the case of the repulsive Hubbard Hamiltonian, there were two motivations for studying both the honeycomb and the π -flux geometries. The first was to verify that the quantum critical transitions to AF order as the on-site repulsion U increases share the same universality class, that of the Gross-Neveu model. The second was to confirm that an intermediate spin-liquid (SL) phase between the semi-metal and AF phases[16], which had been shown not to be present on a honeycomb lattice[17], was also absent on the π -flux geometry.

Studies of the SU(2) π -flux Hubbard model have also been extended to SU(4), using projector QMC[18], and to staggered flux where $\pm\pi$ hopping phases alternate on the lattice[19]. In the former case, the semi-metal to AF order transition was shown to be replaced by a

semi-metal to valence bond solid transition characterized by breaking of a Z_4 symmetry. In the latter work, an intermediate phase with power-law decaying spin-spin correlations was suggested to exist between the semi-metal and AF.

A largely open question is how this physics is affected in the presence of electron-phonon rather than electron-electron interactions. Recent work on the Holstein model[20], which includes an on-site electron-phonon interaction, on the honeycomb lattice suggested a quantum phase transition from semi-metal to gapped Charge-Density Wave (CDW) order [21, 22] similar to the results for the Hubbard Hamiltonian. However, a key difference between the Hubbard and Holstein models is the absence of the SU(2) symmetry of the order parameter in the latter case. Thus, while long range AF order arising from electron-electron interaction occurs only at zero temperature in 2D, the CDW phase transition induced by electron-phonon coupling (EPC) can occur at finite temperature- the symmetry being broken is that associated with two *discrete* sub-lattices.

Here we extend the existing work on the effect of EPC on Dirac fermions from the honeycomb geometry to the π -flux lattice. The π -flux hopping configuration has an additional interesting feature motivating our current work: it is the unique magnetic field value which minimizes the ground state energy for non-interacting fermions at half-filled on a bipartite lattice. Indeed, Lieb has shown that this theorem is also true at finite temperature, and furthermore holds in the presence of Hubbard interactions[23]. Here we consider the thermodynamics of the π -flux lattice with EPC.

This paper is organized as follows: in the next section, we describe the Holstein model and the π -flux square lattice. Section III presents, briefly, a mean-field theory (MFT) for the model. Section IV reviews our primary method, Determinant Quantum Monte Carlo (DQMC). Section V contains results from the DQMC simulations, detailing the nature of the CDW phase transition, both

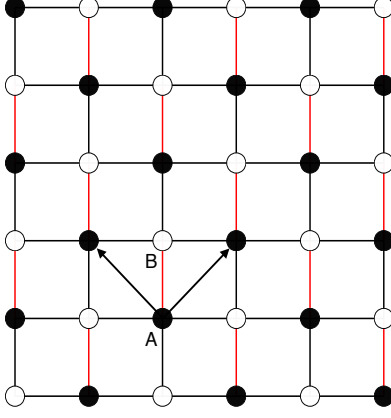


FIG. 1. π -flux phase on a 6×6 square lattice. Sublattices A and B are shown by solid and open circles. Bonds in red correspond to hopping $t' = -t$, as opposite to black lines with hopping t .

the finite temperature transition at fixed EPC, and the quantum phase transition (QPT) which occurs at $T = 0$ with varying EPC. Section VI contains our conclusions.

II. MODEL

The Holstein model [20] describes conduction electrons locally coupled to phonon degrees of freedom,

$$\hat{\mathcal{H}} = - \sum_{\langle \mathbf{i}, \mathbf{j} \rangle, \sigma} (t_{\mathbf{i}, \mathbf{j}} \hat{d}_{\mathbf{i}\sigma}^\dagger \hat{d}_{\mathbf{j}\sigma} + \text{h.c.}) - \mu \sum_{\mathbf{i}, \sigma} \hat{n}_{\mathbf{i}, \sigma} + \frac{1}{2} \sum_{\mathbf{i}} \hat{P}_{\mathbf{i}}^2 + \frac{\omega_0^2}{2} \sum_{\mathbf{i}} \hat{X}_{\mathbf{i}}^2 + \lambda \sum_{\mathbf{i}, \sigma} \hat{n}_{\mathbf{i}, \sigma} \hat{X}_{\mathbf{i}}. \quad (1)$$

The sums on \mathbf{i} and σ run over all lattice sites and spins $\sigma = \uparrow, \downarrow$. $\langle \mathbf{i}, \mathbf{j} \rangle$ denotes nearest neighbors. $\hat{d}_{\mathbf{i}\sigma}^\dagger$ and $\hat{d}_{\mathbf{i}\sigma}$ are creation and annihilation operators of electrons with spin σ on a given site \mathbf{i} ; $\hat{n}_{\mathbf{i}, \sigma} = \hat{d}_{\mathbf{i}\sigma}^\dagger \hat{d}_{\mathbf{i}\sigma}$ is the number operator. The first line of Eq. (1) corresponds to the hopping of electrons, with chemical potential μ . The next line of the Hamiltonian describes dispersionless phonons, local quantum harmonic oscillators of frequency ω_0 and phonon position and momentum operators, $\hat{X}_{\mathbf{i}}$ and $\hat{P}_{\mathbf{i}}$ respectively. The phonon mass M is set to unity. The electron-phonon coupling is included in the last term. We set hopping $t = 1$ as the energy scale and focus on half-filling, ($\langle \hat{n} \rangle = 1$), which can be achieved by setting $\mu = -\lambda^2/\omega_0^2$. It is useful to present results in terms of the dimensionless coupling $\lambda_D = \lambda^2/(\omega_0^2 W)$ which represents the ratio of the effective electron-electron interaction obtained after integrating out the phonon degrees of freedom, and W is the kinetic energy bandwidth.

The two dimensional π -flux phase on a square lattice is schematically shown in Fig. 1. All hopping in the

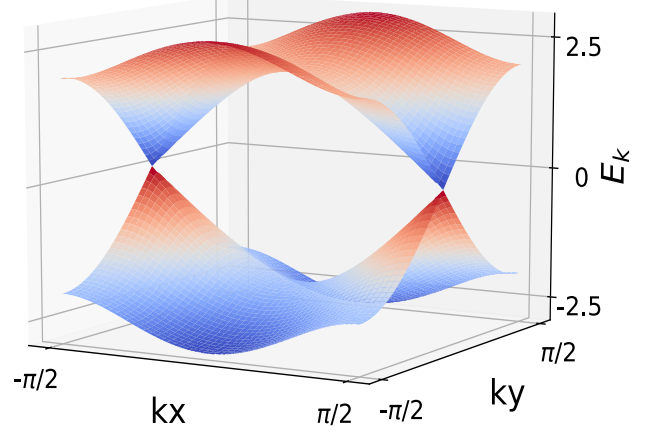


FIG. 2. The dispersion relation $E_{\mathbf{k}}$ for π -flux phase on a square lattice. There are two Dirac points at $(k_x, k_y) = (\pm\pi/2, 0)$.

x direction are t , while half of the hoppings along the y -direction are set to $t' = -t$. As a consequence, a contour around each plaquette picks up a phase of $e^{i\pi}$, corresponding to a magnetic flux of $\Phi_B = \pi$. The lattice is bipartite, with two sublattices A and B. Each unit cell consists of two sites. In reciprocal space, with the reduced Brillouin zone ($|k_x| \leq \pi, |k_y| \leq \pi$), the non-interacting part of Hamiltonian Eq.(1) can be written as,

$$\hat{\mathcal{H}}_0 = \sum_{\mathbf{k}\sigma} \hat{\psi}_{\mathbf{k}\sigma}^\dagger \mathbf{H}_0(\mathbf{k}) \hat{\psi}_{\mathbf{k}\sigma}, \quad (2)$$

where

$$\hat{\psi}_{\mathbf{k}\sigma} = \begin{pmatrix} \hat{d}_{A\sigma} & \hat{d}_{B\sigma} \end{pmatrix}^T, \quad (3)$$

and the noninteracting Hamiltonian matrix

$$\mathbf{H}_0(\mathbf{k}) = \begin{pmatrix} 0 & 2t \cos k_x + 2it \sin k_y \\ 2t \cos k_x - 2it \sin k_y & 0 \end{pmatrix}. \quad (4)$$

The energy spectrum $E_{\mathbf{k}} = \pm 2t \sqrt{\cos^2 k_x + \sin^2 k_y}$ describes a semi-metal with two inequivalent Dirac points at $\mathbf{K}_{\pm} = (\pm\pi/2, 0)$, shown in Fig. 2. In the low-energy regime of the dispersion, the density of states (DOS) vanishes linearly near the Fermi energy, as shown in Fig. 3. The bandwidth of the π -flux phase is $W = 4\sqrt{2}t$. In Fig. 3 the DOS of the honeycomb lattice is shown for comparison. The Dirac Fermi velocity is $v_F = 1.5t$ ($2t$) for the honeycomb (π -flux) lattice. Near the Dirac point, the DOS $\rho(\omega) \sim |\omega|/v_F$, and the π -flux model has a smaller slope.

III. MEAN-FIELD THEORY

In this section, we present a mean-field theory approach to solve the Holstein model. Semi-metal to

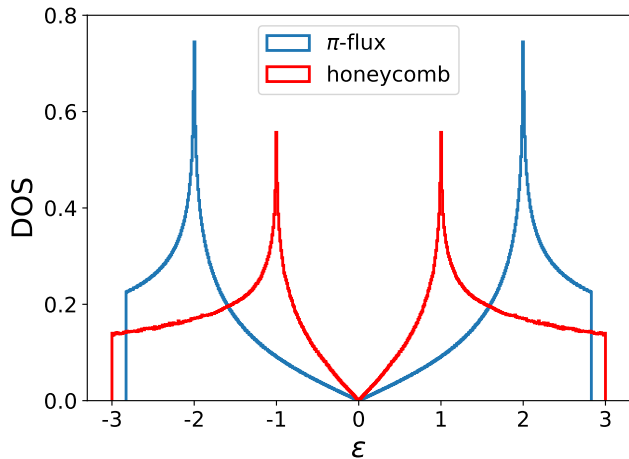


FIG. 3. The density of states (DOS) for the π -flux phase square lattice and the honeycomb lattice. The bandwidths are nearly identical, but the honeycomb lattice has a substantially larger slope of the linear increase of the DOS.

superfluid transitions have previously been investigated with MFT in 2D and 3D [24, 25]. Here we focus on the semimetal to CDW transition. In the mean-field approximation, the phonon displacement at site \mathbf{i} is replaced by its average value, modulated by a term which has opposite sign on the two sublattices,

$$\langle X_{\mathbf{i}} \rangle = X_0 \pm X_{\text{mf}} (-1)^{\mathbf{i}}. \quad (5)$$

Here $X_0 = -\lambda/\omega_0^2$ is the “equilibrium position” at half-filling and X_{mf} is the order parameter. The phonon kinetic energy term is set to zero, i.e. the phonon displacement is assumed to be independent of imaginary-time. The resulting static mean-field Hamiltonian is quadratic in the fermion operators. Diagonalizing gives energy eigenvalues $\epsilon_n(X_{\text{mf}})$. The free energy F can then be directly obtained by,

$$F(\beta, X_{\text{mf}}) = -\frac{1}{\beta} \sum_n \ln(1 + e^{-\beta \epsilon_n}) + \frac{N\omega_0^2}{2}(X_0^2 + X_{\text{mf}}^2), \quad (6)$$

Minimizing the free energy with respect to X_{mf} (or equivalently, a self-consistent calculation) will determine the order parameter. X_{mf} is found to be zero at high temperatures: the energy cost of the second term in Eq. 6 exceeds the energy decrease in the first term associated with opening of a gap in the spectrum ϵ_n . X_{mf} becomes nonzero below a critical temperature T_c .

T_c for the π -flux lattice is shown in Fig. 4, along with the result of analogous MFT calculations for the honeycomb and (zero flux) square geometries. Lattice sizes $L = 180$ is chosen for all three models, sufficiently large to eliminate finite size effects. At zero temperature,

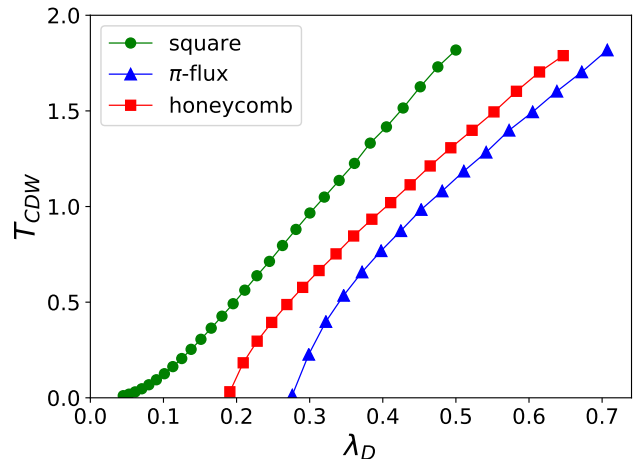


FIG. 4. MFT T_c for CDW phase transition for the square lattice with no magnetic flux, the π -flux phase square lattice, and the honeycomb lattice. For the geometries with a Dirac spectrum MFT captures the existence of a QCP, a critical value of λ_D below which there is no CDW order even at $T = 0$, and the absence of a QCP for the conventional square lattice.

the CDW order exhibits a critical EPC for the π -flux and the honeycomb lattices. This quantum critical point (QCP) arises from the Dirac fermion dispersion, which has a vanishing DOS at the Fermi energy. The honeycomb lattice QCP has a smaller critical value. However, when measured in units of the Fermi velocity, the ratios $\lambda_{D,\text{crit}}/v_F = 0.13(0.14)$ are quite close for the honeycomb(π -flux) geometries. We will see this is also the case for the exact DQMC calculations. For the square lattice, on the other hand, the DOS has a Van-Hove singularity at the Fermi energy, and the CDW develops at arbitrarily small coupling strength.

Another feature of the MFT phase diagram is that, as the coupling increases, T_c increases monotonically. This is in contrast to the exact DQMC results, where T_c decreases at large coupling strengths (Fig. 13). A similar failure of MFT is well known for the Hubbard Hamiltonian: MFT confuses the temperature scale of moment formation, which increases monotonically with U , and the AF ordering scale, which falls as $J \sim t^2/U$.

IV. DQMC METHODOLOGY

We next describe the Determinant Quantum Monte Carlo (DQMC) method[26, 27]. In evaluating the partition function \mathcal{Z} , the inverse temperature β is discretized as $\beta = L_\tau \Delta\tau$, and complete sets of phonon position eigenstates are introduced between each $e^{-\Delta\tau \hat{H}}$. The phonon coordinates acquire an “imaginary time” index, converting the 2-dimensional quantum system to a (2+1) dimensional classical problem. After tracing

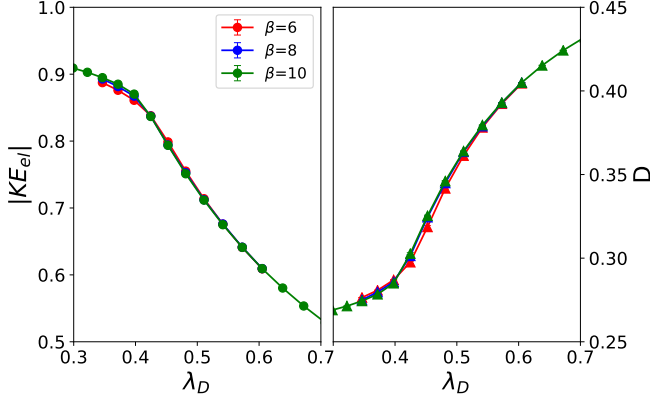


FIG. 5. Left: The magnitude of electron kinetic energy $|\mathcal{K}_{el}|$ as a function of EPC strength λ_D . Simulations are performed on a $L = 10$ lattice at inverse temperatures $\beta = 6, 8, 10$ and fixed $\omega_0 = 1.0$. Right: Double occupancy \mathcal{D} as a function of EPC strength λ_D .

out the fermion degrees of freedom, which appear only quadratically in the Holstein Hamiltonian, the partition function

$$\mathcal{Z} = \int \mathcal{D}x_{i,l} e^{-S_{ph}} [\det \mathbf{M}(x_{i,l})]^2, \quad (7)$$

where the “phonon action”

$$S_{ph} = \Delta\tau \left[\frac{1}{2} \omega_0^2 \sum_i x_{i,l}^2 + \frac{1}{2} \sum_i \left(\frac{x_{i,l+1} - x_{i,l}}{\Delta\tau} \right)^2 \right]. \quad (8)$$

Because the spin up and spin down fermions have an identical coupling to the phonon field, the fermion determinants which result from the trace are the same, and the determinant is squared in Eq. 7. There is no fermion sign problem[28]. We use $\Delta\tau$ small enough so that Trotter errors associated with the discretization of β are of the same order of magnitude as the statistical uncertainty from the Monte Carlo sampling.

V. DQMC RESULTS

Double occupancy and Kinetic Energy

We first show data for several local observables, the electron kinetic energy $|\mathcal{K}_{el}|$ (defined as the first term in the Holstein Hamiltonian) and double occupancy $\mathcal{D} = \langle n_{i\uparrow} n_{i\downarrow} \rangle$. For a tight-binding model on a bipartite lattice at half-filling, Lieb has shown that the energy-minimizing magnetic flux is π per plaquette, both in for noninteracting fermions and in the presence of a Hubbard U [23]. Here we show \mathcal{K}_{el} for the Holstein model, a case not hitherto considered.

Figure 5 shows \mathcal{K}_{el} (left panel) and \mathcal{D} (right panel) as functions of the dimensionless EPC λ_D for $\beta = 6, 8, 10$.

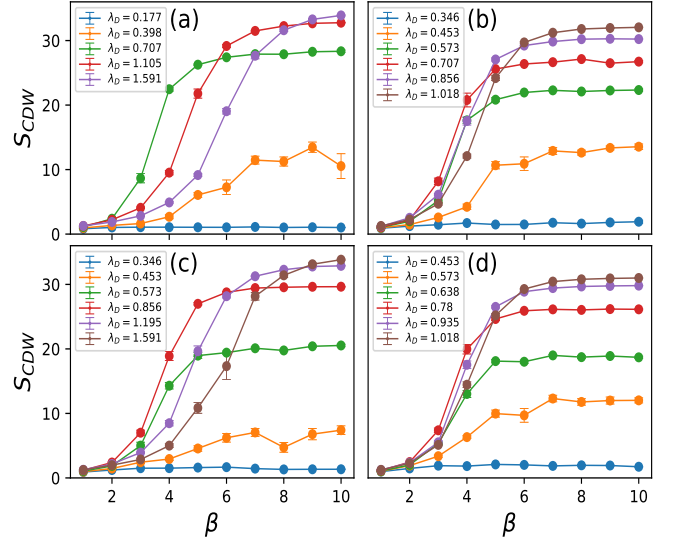


FIG. 6. The CDW structure factor of the π -flux phase Holstein model as a function of inverse temperature β . The phonon frequencies ω_0 are (a), 0.1; (b), 0.5; (c), 1.0; (d), 2.0 in the four panels. The lattice size $L = 6$.

There is little temperature dependence for these local quantities. The magnitude of the kinetic energy $|\mathcal{K}_{el}|$ decreases as λ_D grows, reflecting the gradual localization of the dressed electrons (“polarons”).

At the same time, the double occupancy \mathcal{D} evolves from its noninteracting value $\mathcal{D} = \langle n_{i\uparrow} n_{i\downarrow} \rangle = \langle n_{i\uparrow} \rangle \langle n_{i\downarrow} \rangle = 1/4$ at half-filling, to $\mathcal{D} = 1/2$ at large λ_D . In the strong coupling regime, we expect robust pair formation, so that half of the lattice sites will be empty and half will be doubly occupied.

The evolution of \mathcal{D} and $|\mathcal{K}_{el}|$ have largest slope at $\lambda_D \sim 0.42$ which, as will be seen, coincides with the location of the quantum critical point (QCP) between the semi-metal and CDW phases.

Existence of Long Range CDW Order

The structure factor $S(\mathbf{Q})$ is the Fourier transform of the real-space spin-spin correlation function $c(\mathbf{r})$,

$$S(\mathbf{Q}) = \sum_{\mathbf{r}} e^{i\mathbf{Q} \cdot \mathbf{r}} c(\mathbf{r}),$$

$$c(\mathbf{r}) = \langle (n_{i\uparrow} + n_{i\downarrow})(n_{i+\mathbf{r}\uparrow} + n_{i+\mathbf{r}\downarrow}) \rangle, \quad (9)$$

and characterizes the charge ordering. In a disordered phase $c(\mathbf{r})$ is short-ranged and $S(\mathbf{Q})$ is independent of lattice size. In an ordered phase, $c(\mathbf{r})$ remains large out to long distances, and the structure factor will be proportional to the number of sites, at the appropriate ordering wave vector \mathbf{Q} . At half-filling $S(\mathbf{Q})$ is largest at $\mathbf{Q} = (\pi, \pi)$. We define $S_{cdw} \equiv S(\pi, \pi)$. Figure 6

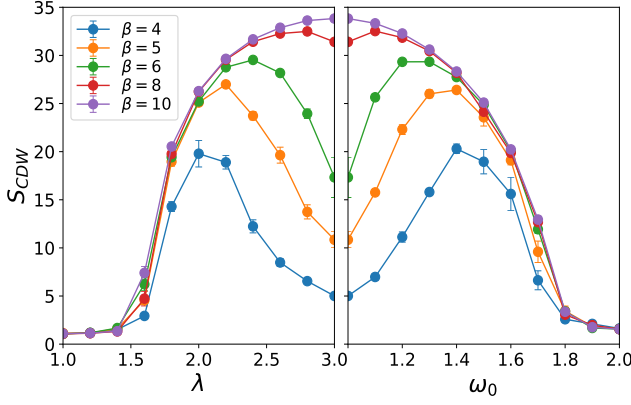


FIG. 7. S_{cdw} (a) as a function of λ at fixed $\omega_0=1.0$; and (b) as a function of ω_0 at fixed $\lambda=3.0$, at different inverse temperatures β . Lattice size $L = 6$ is used in this figure.

displays S_{cdw} as a function of inverse temperature β at different phonon frequencies ω_0 and coupling strengths λ_D . The linear lattice size $L = 6$. At fixed ω_0 and strong coupling, S_{cdw} grows as temperature is lowered, and saturates to $S_{\text{cdw}} \sim N$, indicating the development of long-range order (LRO), i.e. the phase transition into CDW phase.

However, as λ_D is decreased sufficiently, S_{cdw} eventually shows no signal of LRO even at large β , providing an indication that there is a QCP, with CDW order only occurring above a finite λ_D value. Figure 6 also suggests that the critical temperature T_c is non-monotonic with increasing λ_D . The values of β at which S_{cdw} grows first shift downward, but then become larger again. This non-monotonicity agrees with previous studies of Dirac fermions on the honeycomb lattice [21, 22]. We can estimate the maximum T_c to occur at $\lambda_D \approx 0.71, 0.71, 0.86$ and 0.78 for $\omega_0 = 0.1, 0.5, 1.0, 2.0$ respectively. In the anti-adiabatic limit $\omega_0 \rightarrow \infty$, the Holstein model maps onto the attractive Hubbard model, and $T_c = 0$ owing to the degeneracy of CDW and superconducting correlations[29]. (The order parameter has a continuous symmetry.) A recent study[30] has shown that $\omega_0 \gtrsim 10^2 t$ is required to achieve the $-U$ Hubbard model limit, a surprisingly large value.

Figure 7(a) shows S_{cdw} as a function of λ at fixed $\omega_0 = 1.0$. At the highest temperature shown, $\beta = 4$, S_{cdw} reaches maximum at intermediate coupling $\lambda \sim 2.0$, then decreases as λ gets larger. The region for which S_{cdw} is large is a measure of the range of λ for which the CDW ordering temperature T_c exceeds β^{-1} . As β increases, this region is enlarged. Figure 7(b) is an analogous plot of S_{cdw} as a function of ω_0 at fixed $\lambda = 3.0$. The two plots appear as mirror images of each other since the dimensionless EPC $\lambda_D = \lambda^2/(\omega_0^2 W)$ increases with λ , but decreases with ω_0 .

It is interesting to ascertain the extent to which the

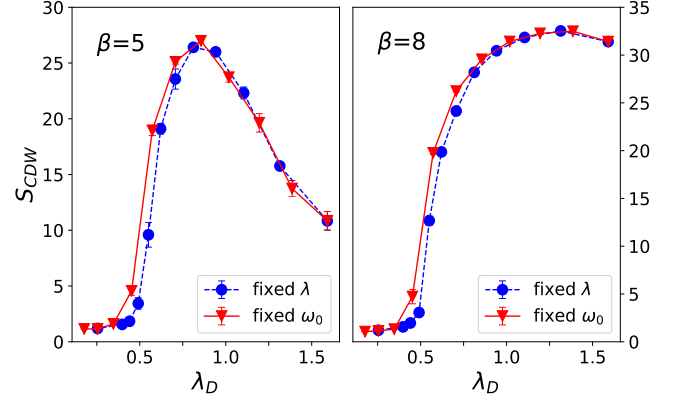


FIG. 8. Comparison of the evolution of S_{cdw} with coupling strength by changing λ or changing ω_0 . Data are taken from Fig. 7(a,b), for $\beta=5$ (left) and $\beta=8$ (right). The difference is negligible at $\lambda_D > 0.8$ but not in the coupling regime $0.4 < \lambda_D < 0.8$ near the QCP. (See Fig. 13.)

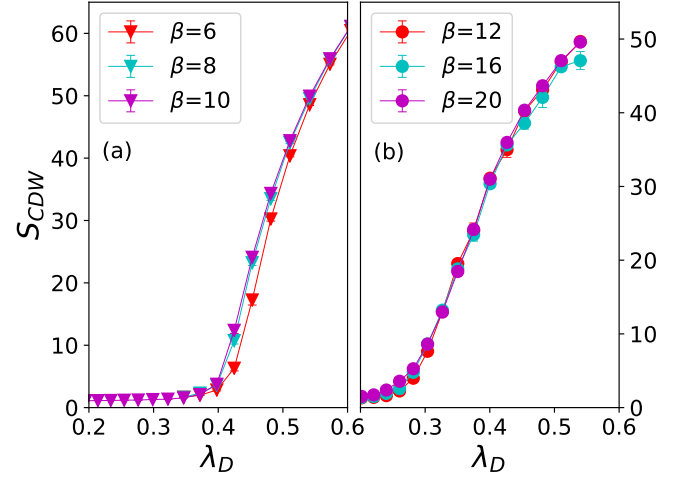


FIG. 9. S_{cdw} as a function of λ_D for π -flux phase square lattice (left) and honeycomb model (right). The lattice size $L = 6$ is used for both geometries. λ_D is varied by changing λ at fixed $\omega_0 = 1.0$. S_{cdw} does not change for the lowest temperatures, indicating that the ground state has been reached for this finite lattice size.

physics of the Holstein Hamiltonian is determined by λ and ω_0 separately, versus only the combination λ_D . Figure 8 addresses this issue by replotting the data of Figs. 7(a,b) as a function of λ_D for two values of the inverse temperature. For $\lambda_D \gtrsim 0.8$, the data collapse well, whereas at small λ_D S_{cdw} can vary by as much as a factor of two even though λ_D is identical. It is suggestive that this disagreement occurs near the region of the QCP. (See Fig. 13.)

We compare the semi-metal to CDW transition with increasing λ_D for the π -flux phase and honeycomb lattices in Fig. 9. These data are at lower temperatures

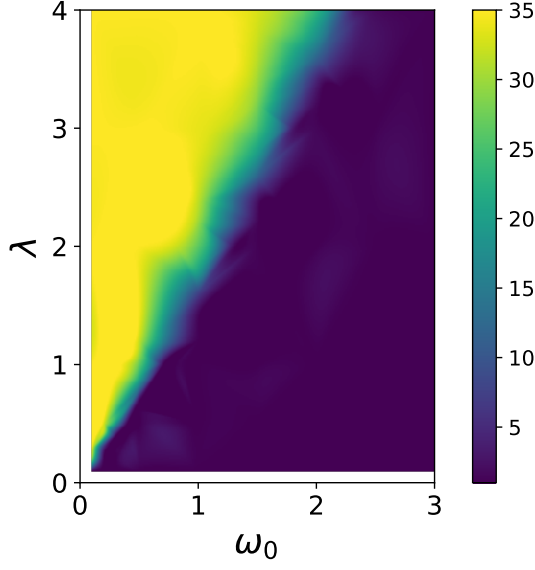


FIG. 10. Heat map of the ground state values of S_{cdw} in the (λ, ω_0) plane.

than those of Fig. 8, so that the ground state values of S_{cdw} have been reached for the system sizes shown.

Ground State in the (λ, ω_0) Plane

Figure 10 provides another perspective on the dependence of the CDW order on λ and ω_0 individually, by giving a heat map of S_{cdw} in the (λ, ω_0) plane at low temperature. The bright yellow in upper-left indicates a strong CDW phase, whereas the dark purple region in lower-right indicates the Dirac semi-metal phase. The phase boundary is roughly linear, as would be expected if only the combination $\lambda_D = \lambda^2/(\omega_0^2 W)$ is relevant. We note, however, that this statement is only qualitatively true. The more precise line graphs of Fig. 8 indicate that along the line $\lambda = \sqrt{\lambda_{D,\text{crit}} W} \omega_0 \sim 1.5 \omega_0$, the separate values of λ and ω_0 are relevant.

Finite Size Scaling: Finite T Transition

A quantitative determination of the finite temperature and quantum critical points can be done with finite size scaling (FSS). Figure 11 gives both raw and scaled data for S_{cdw} for different lattice sizes $L = 4, 6, 8, 10$ at $\lambda = 2.0$, $\omega_0 = 1.0$ as a function of β . Unscaled data are in panel (a): S_{cdw} is small and L -independent at small β (high T) where $c(\mathbf{r})$ is short ranged. On the other hand, S_{cdw} is proportional to $N = L^2$ at large β (low T), reflecting the long-range CDW order in $c(\mathbf{r})$. Panel (b) shows a data crossing for different L occurs when $S_{\text{cdw}}/L^{\gamma/\nu}$ is plotted versus β . A universal

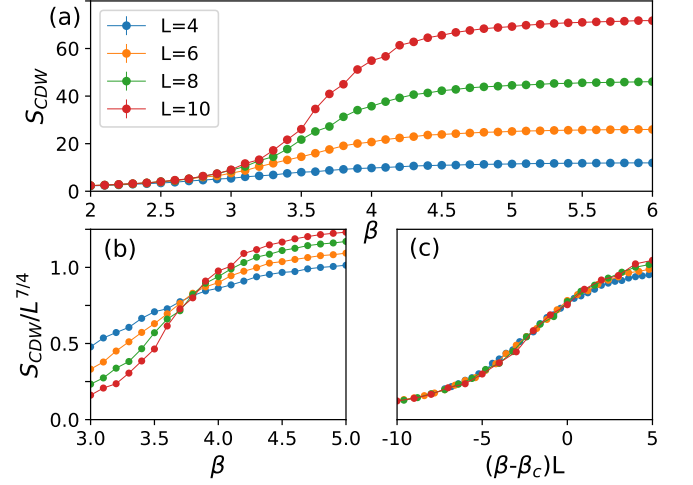


FIG. 11. (a) The CDW structure factor S_{cdw} as a function of β for several lattice sizes. (b) The scaled CDW structure factor $S_{\text{cdw}}/L^{\gamma/\nu}$ as a function of β using Ising critical exponents $\gamma = 7/4$ and $\nu = 1$, showing a crossing of different L at $\beta_c = 3.80$. (c) $S_{\text{cdw}}/L^{\gamma/\nu}$ versus $(\beta - \beta_c)L$, giving a best data collapse at $\beta_c = 3.80$. Here the parameters are $\lambda = 2.0$ and $\omega_0 = 1.0$.

crossing is seen at $\beta \sim 3.80 \pm 0.02$, giving a precise determination of critical temperature T_c . The 2D Ising critical exponents $\gamma = 7/4$ and $\nu = 1$ were used in this analysis, since the CDW phase transition breaks a similar discrete symmetry. Panel (c) shows a full data collapse when the β axis is also appropriately scaled by $L^{1/\nu}$. The best collapse occurs at $\beta_c = 3.80$, consistent with the result from the data crossing.

In the region immediately above the QCP, the DQMC values for T_c are roughly five times lower than those obtained in MFT, and, indeed, the MFT over-estimation of T_c can be made arbitrarily large at strong coupling. This reflects both the relatively low dimensionality ($d = 2$) and the fact that MFT fails to distinguish moment-forming and moment-ordering temperature scales.

Quantum Phase Transition

Analysis of the renormalization group invariant Binder cumulant[31],

$$\mathcal{B} = \frac{3}{2} \left(1 - \frac{1}{3} \frac{\langle S_{\text{cdw}}^2 \rangle}{\langle S_{\text{cdw}} \rangle^2} \right), \quad (10)$$

can be used to locate the quantum critical point precisely. Only lattice sizes $L = 4n$ where n is an integer can be used, for other L the Dirac points are not one of the allowed \mathbf{k} values and finite size effects are much more significant. As exhibited in Fig. 12, for $L = 4, 8$ and 12 , \mathcal{B} exhibits a set of crossings in a range about $\lambda_D \approx 0.4$.

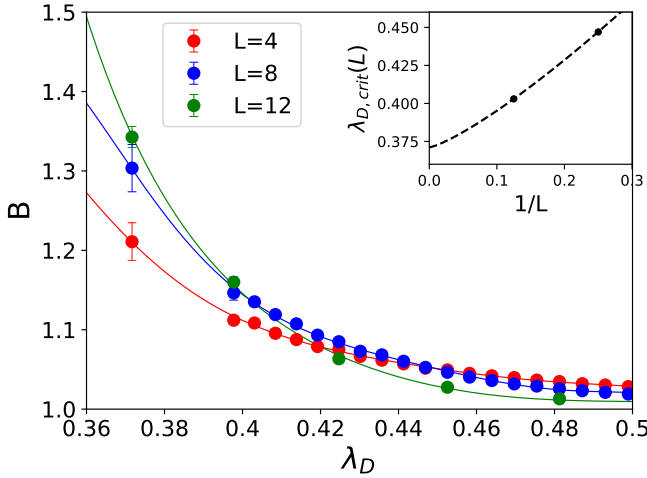


FIG. 12. **Main panel:** Binder cumulant as a function of EPC strength λ_D for three lattice sizes. Inverse temperature is $\beta = 2L$ and ω_0 is fixed at $\omega_0 = 1.0$. **Inset:** Extrapolation of the crossings for pairs of sizes as a function of $1/L$ to get the QCP in the thermodynamic limit.

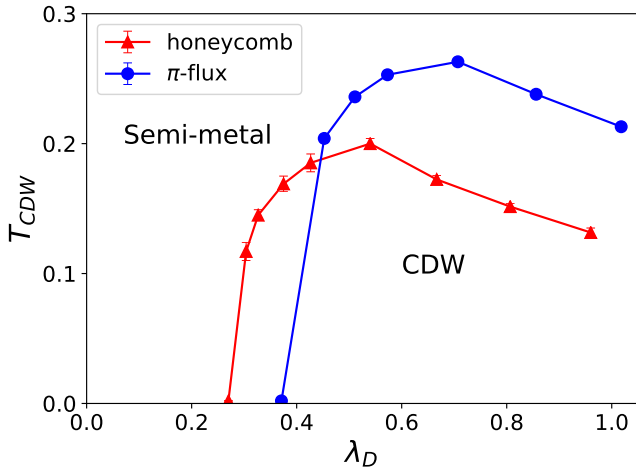


FIG. 13. Critical temperature T_c for CDW phase transition, obtained from DQMC for both π -flux phase square lattice (blue line) and the honeycomb lattice (red line), in a range of coupling strength. λ_D is varied by changing λ at fixed $\omega_0 = 1.0$ for both models. Quantum critical point is determined using Binder cumulant analysis (discussed below). Data for the honeycomb lattice are taken from [21].

An extrapolation in $1/L$, as shown in the inset of Fig. 12, gives $\lambda_{D,crit} = 0.371 \pm 0.003$.

Phase Diagram

Location of the finite temperature phase boundary, Fig. 11, and the QCP, Fig. 12, can be combined into the phase diagram of Fig. 13. Results for the π -flux geometry

(blue circles) are put in better context by compared with those of the honeycomb lattice (red triangles). Data were obtained at fixed $\omega_0 = 1.0$. In both geometries, phase transitions into CDW order happen only above a finite $\lambda_{D,crit}$. Beyond $\lambda_{D,crit}$, T_c rises rapidly to its maximal value before decaying. For π -flux model, T_c reaches a maximum $T_{c,max} \sim 0.26$ at $\lambda_D \sim 0.7$, whereas for the honeycomb lattice T_c reaches its maximum $T_{c,max} \sim 0.20$ at $\lambda_D \sim 0.5$. Similarly $\lambda_{D,crit}$ for π -flux is larger than that of the honeycomb lattice, as $\lambda_{D,crit} = 0.42$ and 0.27 respectively. When measured in terms of the relative Fermi velocities $v_F = 2t, 1.5t$ for the π -flux and honeycomb respectively, these values become very similar: $\lambda_{D,crit}/v_F = 0.21$ and 0.18 for π -flux and honeycomb; $T_{c,max}/v_F = 0.13$ and 0.13 .

VI. CONCLUSIONS

This paper has determined the quantitative phase diagram for Dirac fermions interacting with local phonon modes on the π -flux lattice. A key feature, shared with the honeycomb geometry, is the presence of a quantum critical point $\lambda_{D,crit}$ below which the system remains a semi-metal down to $T = 0$. The values of T_c and $\lambda_{D,crit}$ for the two cases, when normalized to the Fermi velocities, agree to within roughly 10%.

We have also considered the question of whether the properties of the model can be described in terms of the single ratio λ^2/ω_0^2 . We find that qualitatively this is indeed the case, but that, quantitatively, the charge structure factor can depend significantly on the individual values of EPC and phonon frequency, especially in the vicinity of the QCP. However this more complex behavior is masked by the fact that T_c rises so rapidly with λ in that region. In investigating this issue we have studied substantially smaller values of ω_0 than have typically been investigated in QMC treatments of the Holstein Hamiltonian.

Acknowledgments: The work of Y.-X.Z. and R.T.S. was funded by the Department of Energy under Award No. DE-SC0014671. H.G. was supported by NSFC grant No. 11774019. The authors would like to thank B. Cohen-Stead and W.-T. Chiu for useful conversations.

-
- [1] A. H. Castro Neto, F. Guinea, N. M. R. Peres, K. S. Novoselov, and A. K. Geim, *Rev. Mod. Phys.* **81**, 109 (2009).
 - [2] A. Geim, *Science* **324**, 1530 (2009).
 - [3] W. Choi, I. Lahiri, R. Seelaboyina, and Y. S. Kang, *Crit. Rev. in Solid State and Mat. Sci.* **35**, 52 (2010).
 - [4] K. S. Novoselov, V. Fal, L. Colombo, P. Gellert, M. Schwab, K. Kim, *et al.*, *nature* **490**, 192 (2012).

- [5] A. B. Harris, T. C. Lubensky, and E. J. Mele, Phys. Rev. B **40**, 2631 (1989).
- [6] Y. Jia, H. Guo, Z. Chen, S.-Q. Shen, and S. Feng, Phys. Rev. B **88**, 075101 (2013).
- [7] Y. Otsuka and Y. Hatsugai, Phys. Rev. B **65**, 073101 (2002).
- [8] Y. Otsuka, S. Yunoki, and S. Sorella, in *Proceedings of the International Conference on Strongly Correlated Electron Systems (SCES2013)* (2014) p. 013021.
- [9] Z.-X. Li, Y.-F. Jiang, and H. Yao, New J. of Phys. **17**, 085003 (2015).
- [10] F. P. Toldin, M. Hohenadler, F. F. Assaad, and I. F. Herbut, Phys. Rev. B **91**, 165108 (2015).
- [11] Y. Otsuka, S. Yunoki, and S. Sorella, Phys. Rev. X **6**, 011029 (2016).
- [12] T. C. Lang and A. M. Läuchli, arXiv preprint arXiv:1808.01230 (2018).
- [13] H.-M. Guo, L. Wang, and R. Scalettar, Phys. Rev. B **97**, 235152 (2018).
- [14] H. Guo, E. Khatami, Y. Wang, T. P. Devereaux, R. R. Singh, and R. T. Scalettar, Phys. Rev. B **97**, 155146 (2018).
- [15] L. Wang, P. Corboz, and M. Troyer, New J. of Phys. **16**, 103008 (2014).
- [16] Z. Meng, T. Lang, S. Wessel, F. Assaad, and A. Muramatsu, Nature **464**, 847 (2010).
- [17] Y. Otsuka, S. Yunoki, and S. Sorella, J. of Phys.: Conf. Series **454**, 012045 (2013).
- [18] Z. Zhou, C. Wu, and Y. Wang, Phys. Rev. B **97**, 195122 (2018).
- [19] C.-C. Chang and R. T. Scalettar, Phys. Rev. Lett. **109**, 026404 (2012).
- [20] T. Holstein, Annals of Physics **8**, 325 (1959).
- [21] Y.-X. Zhang, W.-T. Chiu, N. C. Costa, G. G. Batrouni, and R. T. Scalettar, Phys. Rev. Lett. **122**, 077602 (2019).
- [22] C. Chen, X. Y. Xu, Z. Y. Meng, and M. Hohenadler, Phys. Rev. Lett. **122**, 077601 (2019).
- [23] E. H. Lieb, Phys. Rev. Lett. **73**, 2158 (1994).
- [24] G. Mazzucchi, L. Lepori, and A. Trombettoni, J. of Phys., B: Atomic, Mol. and Opt. Phys. **46**, 134014 (2013).
- [25] Y.-J. Wu, J. Zhou, and S.-P. Kou, Phys. Rev. A **89**, 013619 (2014).
- [26] R. Blankenbecler, D. J. Scalapino, and R. L. Sugar, Phys. Rev. D **24**, 2278 (1981).
- [27] S. R. White, D. J. Scalapino, R. L. Sugar, E. Y. Loh, J. E. Gubernatis, and R. T. Scalettar, Phys. Rev. B **40**, 506 (1989).
- [28] E. Y. Loh, J. E. Gubernatis, R. T. Scalettar, S. R. White, D. J. Scalapino, and R. L. Sugar, Phys. Rev. B **41**, 9301 (1990).
- [29] R. T. Scalettar, N. E. Bickers, and D. J. Scalapino, Phys. Rev. B **40**, 197 (1989).
- [30] C.-H. Feng, H. Guo, and R. Scalettar, arXiv:1910.09752.
- [31] K. Binder, Z. Phys. B Cond. Mat. **43**, 119 (1981).